A comparison of inelastic electron scattering models based on delta -function representations of the Bethe surface

1992 J. Phys.: Condens. Matter 4 2879

(http://iopscience.iop.org/0953-8984/4/11/015)

J. Phys.: Condens. Matter 4 (1992) 2879–2890. Printed in the UK

A comparison of inelastic electron scattering models based on δ-function representations of the Bethe surface

J M Fernández-Varea†, R Mayol†, F Salvat† and D Liljequist‡

† Facultat de Física (ECM), Universitat de Barcelona, Societat Catalana de Física (IEC), Diagonal 647, 08028 Barcelona, Spain

‡ Department of Physics, University of Stockholm, Vanadisvägen 9, S-113 46 Stockholm, Sweden

Received 23 September 1991, in final form 2 November 1991

Abstract. A comparison is made of the inverse mean free path and stopping power of low- and medium-energy electrons in solids as computed by means of some different simple models of the generalized oscillator strength. The considered generalized oscillator strength models consist of an optical oscillator strength, which is either derived from experimental optical data or modelled from atomic data or from the local plasma approximation, complemented with a suitable algorithm to extend it to the non-zero momentum transfer region. The extension algorithms adopted here are δ-function representations of the Bethe surface similar to the so-called 'one-mode' models of the free-electron gas.

1. Introduction

During the last few years, a number of models to compute inelastic scattering of electrons in solids from knowledge of the optical oscillator strength (OOS) have been proposed. Basically, these approaches are extended versions of the statistical model of Tung *et al* [1] which combines the OOS derived from the local plasma approximation (LPA) [2] with the Lindhard theory for the homogeneous electron gas [3]. Their common characteristic is to model the OOS, and then to extend it into the non-zero momentum transfer region by a convenient and physically motivated recipe—the extension algorithm—thus obtaining a model of the generalized oscillator strength (GOS). Some of these models use extension algorithms of the 'one-mode' or 'plasmon-pole' type, which are attractive primarily since they are simple and, moreover, convenient to use in Monte Carlo simulation. We refer to some of the previous work along these lines: Ritchie and Howie [4], Szajman and Leckey [5], Ashley [6–8], Liljequist [9, 10], Salvat *et al* [11], Penn [12], Tanuma *et al* [13], Ding and Shimizu [14], Martínez *et al* [15], Mayol and Salvat [16] and Mayol *et al* [17]. In the present work, we will consider the low- and medium-energy ($\approx 10^1$–10^4 eV) region.

Usually, the validity of a model is analysed by comparing computed inelastic mean free paths with experimental values. Such a comparison is not completely conclusive since the experimental values are usually determined by the overlayer method which yields attenuation lengths (i.e. including elastic scattering effects) rather than inelastic mean free paths (see, for example [18]). It may also be noted that there seem to be few experimental data on stopping power in the energy region referred to above. This has

0953-8984/92/112879+12$04.50

left open the possibility of some doubt as regards to the choice of the 'best' model. Hence, it is of interest to compare different models for the simulation of inelastic electron scattering. In particular, it is of interest to study in which respect and to what extent the results are sensitive to the adopted OOS and extension algorithm.

Our discussion is based on a well known approach which we state very briefly to establish the notations used here. The inelastic scattering of fast electrons in solids can be computed, to the first-order Born approximation, by means of the atomic differential cross-section [19]

$$\frac{\mathrm{d}\sigma}{\mathrm{d}Q\mathrm{d}W} = \frac{\pi e^4}{E}\frac{1}{WQ}\frac{\mathrm{d}f(Q,W)}{\mathrm{d}W} \tag{1}$$

where $\mathrm{d}f(Q,W)/\mathrm{d}W$ is the GOS. In equation (1), e is the electron charge, E is the incident electron kinetic energy, W is the energy transfer and

$$Q = (\hbar q)^2/2m \tag{2}$$

where $\hbar q$ is the momentum transfer and m the electron mass. We may briefly refer to Q as the 'recoil energy', but it should be noted that it is equal to the recoil energy of the target only in the case where the target is a free electron at rest. In the optical limit $Q = 0$, the GOS reduces to the OOS $\mathrm{d}f(W)/\mathrm{d}W \equiv \mathrm{d}f(Q=0,W)/\mathrm{d}W$. The inverse mean free path (IMFP) λ^{-1} and the stopping power S are given by

$$\lambda^{-1} = N\int_0^E\int_{Q_-}^{Q_+}\frac{\mathrm{d}\sigma}{\mathrm{d}Q\mathrm{d}W}\,\mathrm{d}Q\mathrm{d}W \tag{3}$$

$$S = N\int_0^E\int_{Q_-}^{Q_+}W\frac{\mathrm{d}\sigma}{\mathrm{d}Q\mathrm{d}W}\,\mathrm{d}Q\mathrm{d}W \tag{4}$$

where N is the number of atoms per unit volume in the stopping medium. The integrals extend over the kinematically allowed region of the (Q,W)-plane, i.e.

$$0 \leqslant W \leqslant E \qquad Q_- \leqslant Q \leqslant Q_+ \qquad Q_\pm = \left[E^{1/2} \pm (E-W)^{1/2}\right]^2 . \tag{5}$$

Since here we compare different GOS models with *each other*, we may, for the sake of simplicity, disregard exchange effects.

Starting from equation (1), the modelling of inelastic electron scattering amounts to modelling the GOS. The GOS, or Bethe surface, can be conveniently visualized [19], and may be heuristically interpreted as the 'effective number of atomic electrons' taking part in an inelastic interaction involving a particular energy and momentum transfer. One may, at least roughly, infer the gross features of the GOS from simple physical arguments. For example, it is well known [19] that for large Q the Bethe surface has the shape of a ridge stretched out along the line $W = Q$, corresponding to binary collisions where binding energies are negligible compared with the energy transfer. The shape of the GOS is restricted in particular by the Bethe sum rule [19], i.e.

$$\int_0^\infty \frac{\mathrm{d}f(Q,W)}{\mathrm{d}W}\,\mathrm{d}W = Z \tag{6}$$

where Z is the atomic number of the material.

Alternatively, one may work with the dielectric energy-loss function $\mathrm{Im}(-1/\epsilon)$. The dielectric function $\epsilon(Q,W)$ can be related to the GOS, so that the GOS—which is originally an atomic concept—can be applied to the solid state and to the homogeneous electron gas. In the latter case, it is convenient to refer to the GOS *per electron* rather than per atom, i.e. the Bethe sum rule (6) for the electron gas GOS adds up to unity rather than to the atomic number Z. The OOS is related to the optical limit of $\mathrm{Im}(-1/\epsilon)$ through [20]

$$\frac{\mathrm{d}f(W)}{\mathrm{d}W} = \frac{2W}{\pi\Omega_\mathrm{p}^2} Z\,\mathrm{Im}(-1/\epsilon(W)) \tag{7}$$

where Ω_p is the plasmon energy corresponding to the total average electron density of the stopping material. $\epsilon(W) \equiv \epsilon(Q=0,W)$ is the (complex) dielectric constant.

The computation of inelastic electron scattering in the energy range of interest ($\approx 10^1$–10^4 eV) is far from trivial if one wants to reach an accuracy better than, say, 5–10% in IMFP and stopping power. It is often presumed that the statistical model of Tung *et al* [1] (i.e. the LPA combined with the Lindhard theory [3] for the free-electron gas) should represent a fairly accurate approximation. However, it seems to us that this model is not generally well motivated from a physical point of view, and somewhat ambiguous in its application (cf below) [2,17]. In particular, it does not yield a proper threshold for bound-shell ionization [16]. Moreover, this kind of approach appears not to be well suited to convenient application in Monte Carlo simulations. We will therefore also consider some alternatives.

The paper is structured as follows. As stated before, our basic approach is to model the OOS, and then to extend it into the $Q > 0$ region using a suitable algorithm, thus obtaining a model of the GOS. The OOS models adopted in our calculations are described in section 2. Three extension algorithms are presented in section 3. In section 4, IMFPs and stopping powers in aluminium and copper computed from different combinations of OOS and extension algorithm are shown. Finally, conclusions are summarized in section 5.

2. Modelling the OOS

Following Penn [12], one may expect that an experimentally well-determined OOS should be the most reliable to be found. It may however not always be available, so one should also look for other methods to obtain an estimate of the OOS. Also, it may turn out (cf below) that the OOS does not, in practice, need to be specified in very great detail, or with high accuracy in every detail. As compared to extensive tabulations, a simpler representation in terms of a few parameters might be possible and sometimes even more convenient. We will compare results from the following three OOS models.

2.1. OOS model I. Experimental OOS

Experimental optical data tables, i.e. tabulations of the dielectric constant $\epsilon(W)$ or the refractive index and damping coefficient, are currently available for selected materials [21]. The experimental OOSs for aluminium and copper are shown in figure 1.

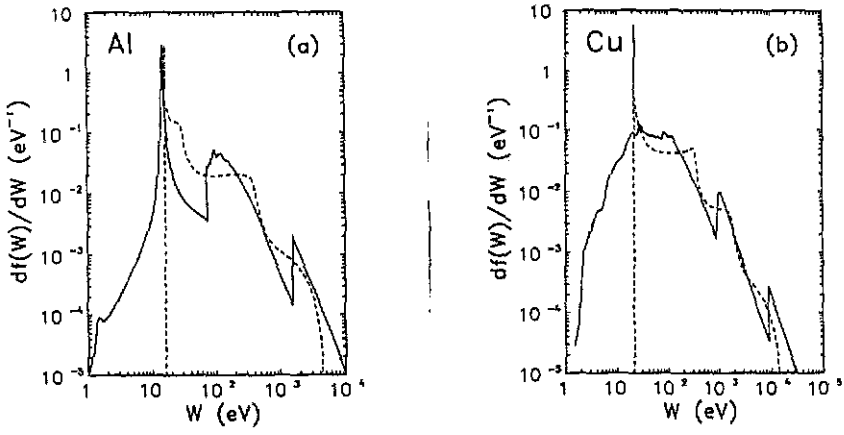

Figure 1. OOSs computed from experimental optical data [21] (full curves) and obtained from the LPA (equation (11)) with Dirac–Hartree–Slater atomic densities (broken curves) for Al (a) and Cu (b).

These have been obtained numerically [17] according to equation (7) using the optical functions tabulated in reference [21].

The mean ionization potential I, which is the basic parameter in the high-energy Bethe stopping power formula, can be obtained from the OOS as

$$Z \ln I = \int_0^\infty \ln W \, \frac{\mathrm{d}f(W)}{\mathrm{d}W} \, \mathrm{d}W \,. \tag{8}$$

Making a linear extrapolation of the K-edge slope in a log–log diagram, the experimental OOSs in figure 1 lead to $I = 164.5$ eV for aluminium and $I = 321.0$ eV for copper. These values are in excellent agreement with those recommended by Berger and Seltzer [22].

2.2. OOS model II. Local plasma approximation

An alternative is the LPA, which amounts to assuming that the OOS for a single-element scattering medium, whose atoms have a locally varying atomic electron density $\rho(r)$, can be obtained by considering that the response of the electrons in a volume element $\mathrm{d}v$ at r is the same as if they were in a free-electron gas of density $\rho(r)$. Neglecting plasmon damping, the OOS for a free-electron gas (FEG) of density ρ reduces to the delta function

$$\left(\frac{\mathrm{d}f(W)}{\mathrm{d}W}\right)_{\mathrm{FEG}} = \delta\left[W - W_{\mathrm{pl}}(\rho)\right] \tag{9}$$

where

$$W_{\mathrm{pl}}(\rho) \equiv \left(4\pi\rho\hbar^2 e^2/m\right)^{1/2} \tag{10}$$

is the long-wavelength limit of the plasmon energy. Therefore, the LPA leads to the following OOS

$$\left(\frac{\mathrm{d}f(W)}{\mathrm{d}W}\right)_{\mathrm{LPA}} = \int_0^{r_{\mathrm{WS}}} \rho(r)\, \delta\{W - \gamma W_{\mathrm{pl}}[\rho(r)]\}\, 4\pi r^2 \, \mathrm{d}r \tag{11}$$

where r_{WS} is the Wigner–Seitz radius. In the calculations reported below, we have used atomic electron densities obtained from Dirac–Hartree–Slater calculations with Wigner–Seitz boundary conditions. It turns out that the plasmon energy may have to be adjusted for the results to agree with higher energy stopping power theory and relevant experimental data (i.e. the Bethe formula and the mean ionization potential I). The parameter γ is introduced in order to obtain the correct mean ionization potential as derived, for instance, from accurate experimental optical data. In this way, it is guaranteed that the high-energy stopping power derived from the OOS (11) will agree with the stopping power given by the Bethe formula (using the same I value). The values of this parameter, as derived from the mean ionization potential computed from the experimental OOS, are $\gamma = 1.31$ for aluminium and $\gamma = 1.26$ for copper. The OOSs (11) for these two materials are included in figure 1 for comparison purposes. It is seen that the OOS derived from the LPA may be notably different from the OOS obtained from optical data. The fact that γ deviates appreciably from unity also points to the *ad hoc* and somewhat unsatisfying nature of the LPA. Moreover, it may be noted that the choice of γ is not unambiguous, since a value of unity, rather than the above values, should be chosen to reproduce the IMFP obtained from optical data [17].

2.3. OOS model III. Subshell oscillator models

As a second alternative, one may suggest that a model of the OOS may be constructed from atomic shell or band-structure data, e.g. using atomic configuration and binding energies [9–11]. This may (as in the LPA case) require the adjustment of some parameters (see [9, 10]) to get agreement with empirical results, e.g. with the mean ionization potential. A systematic procedure for this purpose is to use regularly-shaped oscillator distributions to model the well-determined experimental OOS in terms of contributions from different subshells, bands and collective excitations. We will refer to this as "subshell oscillator models". An argument for this seemingly retrograde procedure is, as mentioned above, that one purpose apart from that of accuracy must be to find algorithms and data sets which are comparatively easy to perform, store and convey, to implement into Monte Carlo routines, and to generalize to new cases. In fact, since we can see [17] that the OOS corresponding to the LPA actually differs appreciably from the experimental OOS, and nevertheless works rather well, we may expect that an appropriately constructed subshell oscillator distribution, expressed in terms of a limited number of material-dependent parameters, should work even better. Such a model may, in turn, provide indications as to what recipe one should use to extrapolate to cases for which the experimental OOS is not available.

Henceforward we will make use of the fact that formally, as well as in the practice of computer calculations, the OOS might be represented as a sum of suitably spaced 'optical' oscillators $\delta(W - W_j)$, i.e.

$$\frac{\mathrm{d}f(W)}{\mathrm{d}W} = \sum h_j \delta(W - W_j) \tag{12}$$

where h_j is the oscillator strength associated with energy transfer W_j. For the sake of illuminating the extent to which the OOS must be precisely specified, we will, as regards subshell oscillator models, limit our considerations mainly to the simplest model of this kind, which consists of a set of a few optical oscillators $\delta(W - W_{sh})$, each representing, in a very crude way, optical excitations from a particular atomic

shell [9]. W_{sh} is the excitation energy (which may also be regarded as the partial mean ionization potential for this shell [9]). Here we set the associated oscillator strength h_{sh} equal to the number of electrons in that shell. The excitation energy W_{sh} of each inner shell is set proportional to the corresponding binding energy U_{sh}, i.e. $W_{sh} = aU_{sh}$ where a is an adjustable parameter. The excitation energy $W_{v\,sh}$ of the $h_{v\,sh}$ valence electrons is estimated separately, e.g. from a free-electron gas approximation, from low energy loss data, or so as to get agreement with the empirical IMFP [9]. The parameter a is then determined from the equation

$$Z \ln I = h_{v\,sh} \ln(W_{v\,sh}) + \sum h_{sh} \ln(aU_{sh}) \tag{13}$$

so that the OOS (12) gives the same mean ionization potential as the experimental OOS. Consequently, we expect the three OOS models to give converging results on stopping power at high energies. The presently used model III parameters for aluminium and copper are given in table 1.

Table 1. OOS model III parameters for aluminium and copper. The present values of the parameter a (see equation (13)) for Al and Cu are 2.27 and 2.39 respectively.

	Aluminium			Copper		
	h_{sh}	U_{sh} (eV)	W_{sh} (eV)	h_{sh}	U_{sh} (eV)	W_{sh} (eV)
Inner-shell electrons	2	1560	3536.2	2	8979	21455.8
	2	118	267.5	2	1096	2619.0
	6	73.5	166.6	6	937	2239.0
				2	120	286.8
				6	74	176.8
Valence electrons	3	—	15.0	11	—	50.0

In more accurate subshell oscillator models [10,15], optical excitations of a particular shell (or subshell) are represented by an oscillator *distribution* $\sum h_j \delta(W - W_j)$, where $\sum h_j = h_{sh}$. For inner shells, one should have, approximately, $h_j \propto W_j^{-\alpha}$ for energies W_j above the ionization threshold, where the exponent α is directly related to the parameter a and may be estimated from basic photoelectric theory [9,10]. From such theory, one would in general expect a to have values in the range ≈ 1.5–2.0, as discussed in reference [9]. The values in the present case are appreciably higher (see table 1). For copper (and other transition metals), this is essentially due to the use of a single oscillator for the valence electrons, which tends to enforce an unnaturally low value of the partial mean ionization potential [9] of the outermost (valence) shell. For aluminium, it appears that the rather high value of a may be partly appropriate, being due to the particular structure of the OOS near the L-shell edge (see figure 1(a)). This indicates that the use of a single proportionality constant a, as in equation (13), might be somewhat crude.

3. Extension of OOS to GOS

On the basis of equation (12) it is convenient to extend the OOS into the $Q > 0$ region, i.e. into the GOS, by means of a device referred to as 'δ-oscillators' [10]. These

extensions include the well known 'one-mode' or 'plasmon-pole' models. A δ-oscillator is basically defined as the function $\delta(W - F_j(Q))$, where the dispersion relation $F_j(Q)$ is a single-valued function of the recoil energy Q. In the optical limit, the δ-oscillator reduces to an optical oscillator with $W_j = F_j(0)$. The extension of the OOS to the GOS is carried out simply by replacing each optical oscillator by a δ-oscillator. Thus equation (12) is replaced by

$$\frac{\mathrm{d}f(Q,W)}{\mathrm{d}W} = \sum h_j \delta(W - F_j(Q)) \,. \tag{14}$$

Parenthetically, it may be noted that one can always use δ-oscillators to extend the OOS into the GOS. To see this, replace for the moment $F_j(Q)$ by a function $F(W';Q)$, where W' is a continuous variable representing energy transfer at $Q = 0$, and let $F(W';Q)$ be defined by

$$\int_0^{W'} \frac{\mathrm{d}f(W)}{\mathrm{d}W}\,\mathrm{d}W = \int_0^{F(W';Q)} \frac{\mathrm{d}f(Q,W)}{\mathrm{d}W}\,\mathrm{d}W \,. \tag{15}$$

Then it can be shown that

$$\frac{\mathrm{d}f(Q,W)}{\mathrm{d}W} = \int_0^{\infty} \frac{\mathrm{d}f(W')}{\mathrm{d}W'}\,\delta(W - F(W';Q))\,\mathrm{d}W' \,. \tag{16}$$

This means that the GOS can be expressed as the OOS extended by δ-oscillators along curves $F(W';Q)$ in the (Q,W)-plane, such that a summation as in the Bethe sum rule (6) gives a constant value along each curve.

However, the present models employ δ-oscillators with simple and schematic dispersion relations $F_j(Q)$. The main reason for using δ-oscillators is that we find them convenient for modelling and simulation purposes. An alternative to the use of δ-oscillators is, for example, extension by means of the complete Lindhard dielectric function for the free-electron gas (see e.g. reference [1]), or by means of Drude-type simplifications of the Lindhard dielectric function [4, 12–14].

We consider, then, the physically motivated choice of δ-oscillators for different purposes—namely, for the excitation of valence electrons, and for the excitation of inner-shell electrons. Here we will compare three particularly simple δ-oscillator models, named, for brevity, the plasmon (line) (P) model, the (inner) shell (S) model, and the two-modes (T) model. A common simplifying feature is that the dispersion relations $F_j(Q)$ are linear or piecewise-linear which, for example, agrees well with physical reality along the Bethe ridge.

3.1. Plasmon (P) model

This model has been used e.g. by Ashley [6–8]. It is given by

$$F_j(Q) = W_j + Q \tag{17}$$

where W_j is the optical limit. This relation is actually a schematic simplification of the plasmon dispersion relation for a free-electron gas [6], extended into a line parallel to (and, for large Q, effectively close to) the asymptotic middle of the Bethe ridge. When this model is used to describe bound-shell ionization, however, it shifts the ionization threshold to $2U_{\mathrm{sh}}$ [16]. The P model, or its more accurate version using the proper low-Q plasmon dispersion relation [12], is so far the most extensively used of the three models discussed here.

3.2. Shell (S) model

The shell model is defined by

$$F_j(Q) = W_j \qquad Q \leqslant W_j$$
$$F_j(Q) = Q \qquad Q > W_j \,. \tag{18}$$

The physical picture here is that the interaction typically has either 'resonance' character or 'free' (binary) character, corresponding to distant and close collisions, respectively [23]. The behaviour for $Q > W_j$ corresponds to the Bethe ridge.

The S model has been tried for the free-electron gas [9], taking the plasmon energy as the excitation energy W_j. In this case, it fails at incident electron energies about and below the plasmon excitation threshold, a fault shared to some extent with the P model. It has recently been proposed [16] that the S model is more satisfactory than the P model for inner-shell ionization, and that it yields fairly accurate ionization cross-sections when used together with an experimental OOS or an OOS derived from hydrogenic wavefunctions [16].

3.3. Two-modes (T) model

The T model described here is a slight simplification of a model described in more detail elsewhere [15, 17]. It is designed to reproduce the results of the Lindhard theory [3] for the free-electron gas, and has been shown to be an improvement over the P model in this respect [15]. Like the Lindhard theory and the statistical model of reference [1] it is thus well suited to valence electrons. When used to describe bound-shell ionization, it predicts energy losses below the ionization threshold, and the plasmon branch (see below) creates, like the P model, an extra threshold at $2U_{sh}$.

The present T model is obtained if in equation (14) we replace the single-mode δ-oscillators $\delta(W - F_j(Q))$ by

$$[1 - g_j(Q)]\delta(W - (W_j + Q)) + g_j(Q)\delta(W - Q) \tag{19}$$

where

$$g_j(Q) \equiv \min\left(1, \frac{AQ^3}{W_j^2\,(W_j + Q)}\right) . \tag{20}$$

The parameter A is chosen so as to optimize quantitative agreement with the Lindhard theory. Within a limited region of small Q, two excitation modes coexist. One mode or branch, with strength $1 - g_j(Q)$, represents plasmon excitation; the other, with strength $g_j(Q)$, represents electron–hole excitation. For large Q, $g_j(Q) = 1$, i.e. the plasmon branch disappears, and the electron–hole excitation branch continues into the Bethe ridge. For small Q, $g_j(Q)$ decreases to zero roughly as Q^3; thus the strength of the plasmon branch increases to a maximum. In this way, the T model reflects the two major and related aspects of the collective behaviour of the electron gas, i.e. the screening of the Coulomb interaction and the occurrence of plasma oscillations. In equation (19), the plasmon branch has, for simplicity, the inclination unity ($dW/dQ = 1$). Actually, the inclination depends on the plasmon energy. This should be taken into account to reproduce closely the results of the Lindhard theory [15]. Further details and the explicit form of the parameter A are discussed elsewhere [15].

4. Comparison of different OOS and extension models

We present here examples of the magnitude and character of the differences which arise in the inelastic IMFP λ^{-1} and the stopping power S when the OOS models I–III are used in various combinations with the P, S and T δ-oscillator models performing the extension from OOS to GOS.

Figure 2 compares the three extension algorithms P, S and T when used to compute the IMFP and stopping power of electrons moving in a free-electron gas (OOS model III with a single oscillator, according to equation (9)). The consideration of electron gases with very high densities, i.e. with high W_{pl} values, is required for the LPA description of inner-shell ionization. Stopping powers agree well except near and below the plasmon threshold. The IMFP computed by the P model is systematically somewhat smaller than the IMFP computed by the T model, while for the S model it is somewhat larger. This is a typical result, which is seen again in the following.

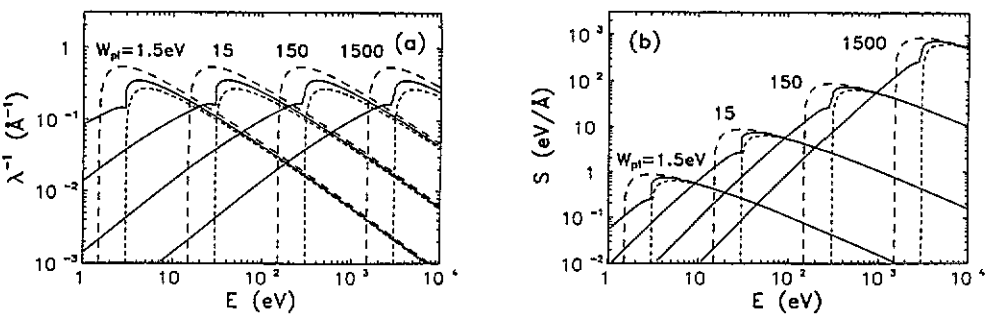

Figure 2. Comparison of inverse mean free path (a) and stopping power (b) in free-electron gases of different densities, computed with the P (short-dashed broken curves), S (long-dashed broken curves) and T (full curves) δ-oscillator models. The energy loss (non-zero loss, in case of the T model) at $Q = 0$ is the long-wavelength plasmon energy W_{pl}. The considered gases have plasmon energies of 1.5, 15, 150 and 1500 eV.

Figures 3 and 4 show a comparison between the results of the P, S and T models when combined with the experimental OOS for aluminium and copper. Since the T model is physically suited to the valence electrons, which dominate the results for stopping power as well as IMFP (in particular at low energy), we expect the T model to be the most accurate *single* choice here. The S model is presumably better than the T model to describe inner-shell excitations, but the relative contribution from inner shells to the IMFP and stopping power is small. The S model gives a slightly larger and the P model a slightly smaller stopping power, as compared to the T model. The difference in IMFP is similar but somewhat larger. These results can evidently be understood from the results for the free-electron gas (cf figure 2). It may be noted that in the results obtained by means of the experimental OOS for copper, the familiar plasmon threshold obtained with the LPA OOS (cf figure 5 below) is entirely absent; there is no sharp, well-defined plasmon in copper. That it arises in the LPA is apparently an artifact of that method.

IMFP and stopping power in copper, obtained from the LPA OOS with the three extension algorithms, are shown in figure 5. The threshold for non-zero IMFP and stopping power with the P and S models evidently corresponds to the effectively lower

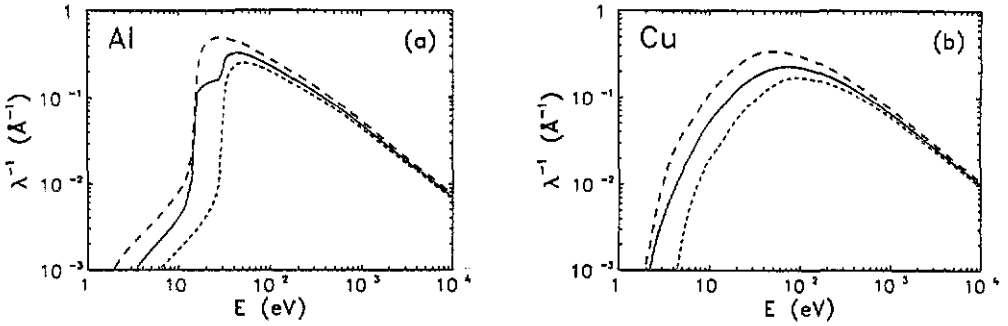

Figure 3. Inverse mean free path in Al (a) and Cu (b) computed from OOS model I (experimental OOS) using the P (short-dashed broken curves), S (long-dashed broken curves) and T (full curves) δ-oscillator models.

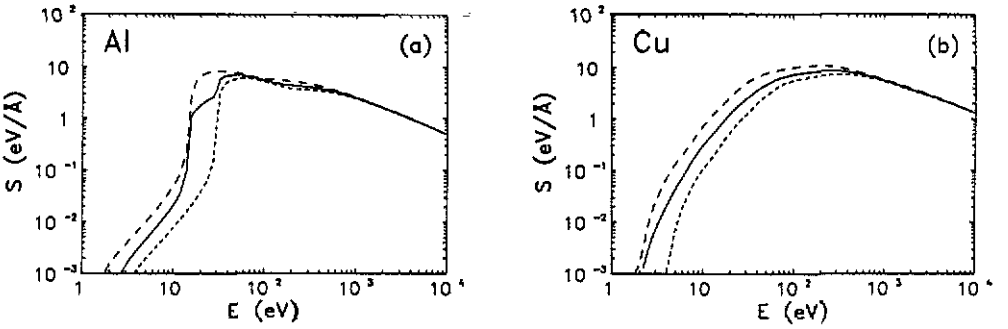

Figure 4. Stopping power in Al (a) and Cu (b) computed from OOS model I (experimental OOS) using the P (short-dashed broken curves), S (long-dashed broken curves) and T (full curves) δ-oscillator models.

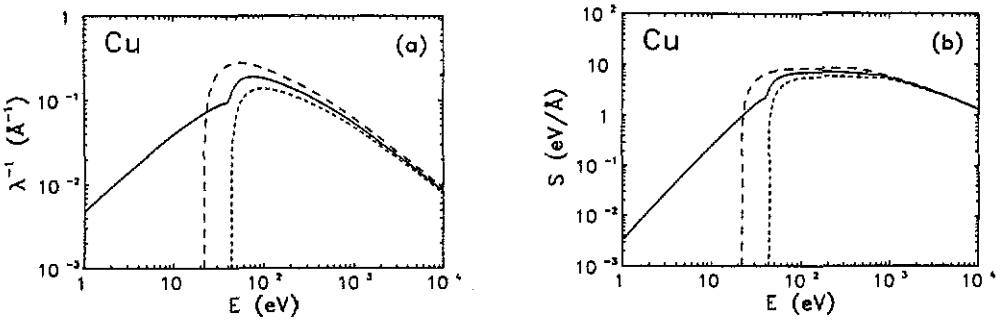

Figure 5. Inverse mean free path (a) and stopping power (b) in Cu, computed from OOS model II (LPA) using the P (short-dashed broken curves), S (long-dashed broken curves) and T (full curves) δ-oscillator models.

limit of the plasmon energy found with the LPA (cf figure 1). The relative differences above threshold are similar to those observed in figures 3 and 4.

In figures 2–5 we have compared the three δ-oscillator models P, S and T with *each other*, assuming the same OOS for them all (either the one corresponding to a free-electron gas, or the one derived from experimental optical data—model I—or from the LPA—model II). In figures 6 and 7 below we will compare the results of different

OOSs—models I, II and III—restricting ourselves, for clarity, to the T model to extend these to $Q > 0$.

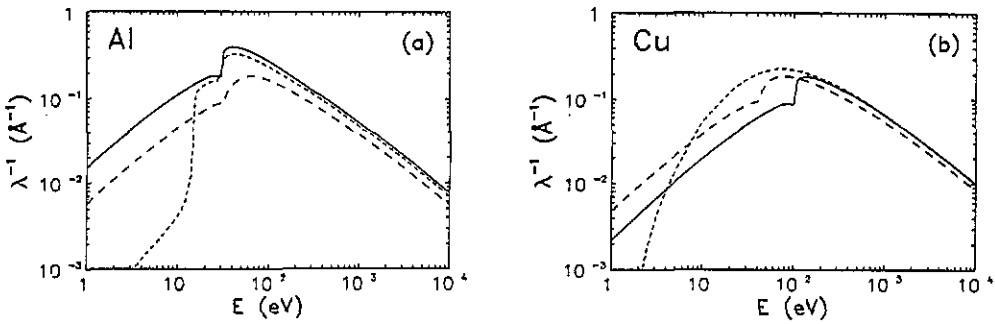

Figure 6. Inverse mean free path in Al (a) and Cu (b) computed from OOS models I (experimental OOS, short-dashed broken curves), II (LPA, long-dashed broken curves) and III (subshell oscillator model, full curves) with the T δ-oscillator model.

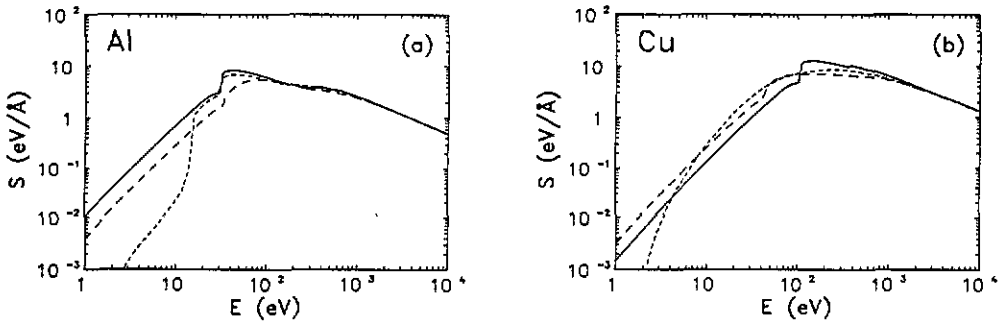

Figure 7. Stopping power in Al (a) and Cu (b) computed from OOS models I (experimental OOS, short-dashed broken curves), II (LPA, long-dashed broken curves) and III (subshell oscillator model, full curves) with the T δ-oscillator model.

IMFPs and stopping powers in aluminium and copper, computed by the T extension algorithm with the three OOS models, are shown in figures 6 and 7. For aluminium, the results from OOS models I and III are in quite good agreement on the whole energy range, despite the crudeness of model III. This is apparently due to the fact that the use of a single oscillator for the valence electrons in aluminium is actually appropriate (it corresponds realistically to the dominant bulk plasmon typical of this metal). The use of a single oscillator for each inner shell is a fairly good approximation as far as IMFP and stopping power are concerned; actually, this approximation is effectively equivalent to that used by Powell [24].

For copper, we also find (as expected) a good agreement in stopping power for models I and III at high energies, and, with present parameter values, fortuitously also in the IMFP. The use of a single oscillator for the valence electrons in copper is, however, not appropriate: it leads to a large discrepancy in the IMFP at energies below about 10^2 eV, and to a somewhat excessive stopping power at energies between 10^2 and 10^3 eV. Preliminary calculations indicate that the valence electrons in copper are well represented by a very broad oscillator distribution (from about 10 eV to a few hundred eV). The inner shells can still be approximately represented by single oscillators.

5. Conclusions

Certain results, e.g. the IMFP and stopping power at low energies and the IMFP at somewhat higher energies, are quite sensitive to the model used to extend the adopted OOS into the GOS. A preliminary conclusion is that a combination of the two-modes (T) model (for valence electrons) and the shell (S) model (for inner shells) could be a convenient recipe for simulation purposes. The OOS may be obtained directly from optical data, when those are available. However, our results also lead us to expect that a modelling of tabulated OOS in terms of atomic and band-structure data may be worthwhile, and could make it possible to estimate the OOS from atomic data with sufficient accuracy to obtain results that are quite comparable to the LPA, or even a substantial improvement beside this last approximation.

One may expect a further improvement by introducing subshell oscillator distributions rather than single oscillators, and taking into account exchange effects and corrections to the Born approximation [16,25] at low energies.

Acknowledgments

Financial support from the Comisión para la Investigación Científica y Técnica (Spain), project no PB86-0589, is gratefully acknowledged. F Salvat wishes to express his gratitude to the Servicio de Cooperación Científico-Técnica of the Spanish Ministerio de Asuntos Exteriores for a travel grant.

References

[1] Tung C J, Ashley J C and Ritchie R H 1979 *Surf. Sci.* **81** 427
[2] Johnson P E and Inokuti M 1983 *Commun. At. Mol. Phys.* **14** 19
[3] *Lindhard J 1954 K. Danske Vidensk. Selsk. Mat. - Fys. Medd.* **28** 1
[4] Ritchie R H and Howie A 1977 *Phil. Mag.* **36** 463
[5] Szajman J and Leckey R C G 1981 *J. Electron. Spectrosc. Relat. Phenom.* **23** 83
[6] Ashley J C 1982 *J. Electron. Spectrosc. Relat. Phenom.* **28** 177
[7] Ashley J C 1988 *J. Electron. Spectrosc. Relat. Phenom.* **46** 199
[8] Ashley J C 1990 *J. Electron. Spectrosc. Relat. Phenom.* **50** 323
[9] Liljequist D 1983 *J. Phys. D: Appl. Phys.* **16** 1567
[10] Liljequist D 1985 *J. Appl. Phys.* **57** 657
[11] Salvat F, Martínez J D, Mayol R and Parellada J 1985 *J. Phys. D: Appl. Phys.* **18** 299
[12] Penn D R 1987 *Phys. Rev.* B **35** 482
[13] Tanuma S, Powell C J and Penn D R 1988 *Surf. Interface Anal.* **11** 577
[14] Ding Z -J and Shimizu R 1989 *Surf. Sci.* **222** 313
[15] Martínez J D, Mayol R and Salvat F 1990 *J. Appl. Phys.* **67** 2955
[16] Mayol R and Salvat F 1990 *J. Phys. B: At. Mol. Phys.* **23** 2117
[17] Mayol R, Fernández-Varea J M, Salvat F and Liljequist D 1991 *Interaction of Charged Particles with Solids and Surfaces* NATO ASI Series vol B-271, ed A Gras-Martí *et al* (New York: Plenum) pp 585–591
[18] Jablonski A and Tougaard S 1990 *J. Vac. Sci. Technol.* A **8** 106
[19] Inokuti M 1971 *Rev. Mod. Phys.* **43** 297
[20] Fano U 1963 *Ann. Rev. Nucl. Sci.* **13** 1
[21] Palik D (ed) 1985 *Handbook of Optical Constants of Solids* (New York: Academic)
[22] Berger M J and Seltzer S M 1983 *National Bureau of Standards Report* NBSIR 82-2550-A
[23] Bohr N 1948 *K. Danske Vidensk. Selsk. Mat. - Fys. Medd.* **18** 1
[24] Powell C J 1974 *Surf. Sci.* **44** 29
[25] Hippler R 1990 *Phys. Lett.* **144A** 81